

Optical conductivity in the t - J model: Slave-boson, large- N technique

Yunkyu Bang

Max-Planck-Institut für Festkörperforschung, Heisenbergstrasse 1, 7000 Stuttgart 80, Germany

G. Kotliar

Serin Physics Laboratory, Rutgers University, Piscataway, New Jersey 08855-0849

(Received 16 March 1993; revised manuscript received 6 July 1993)

We study the real part of the optical conductivity in the t - J model using the slave-boson technique and the large- N expansion to the next-to-leading order in $1/N$. The conductivity falls off at a slower rate than predicted by the Drude theory due to the coupling to the low-energy spin excitation. The absorptions from the mid-infrared (MIR) range to higher frequency (~ 1 eV) arise from the incoherent motion of the charge carrier. We compare our results to finite-cluster exact-diagonalization studies and to experimental studies in the copper oxide system.

The optical conductivity is an established probe of electronic structure. Measurements of this quantity in the cuprate superconductors are interpreted to show a genuine strong correlation effect. Two main features of the experimental data in the Y-Ba-Cu-O (YBCO) (Ref. 1) and in the La-Sr-Cu-O system² are (1) a slow drop of the low-frequency absorption, indicating a scattering rate proportional to $\sim w$ in contrast to the ordinary Drude form with constant scattering rate and (2) broad mid-infrared (MIR) structures starting at around 500 cm^{-1} . The slower decay of the low-frequency absorption is understood as a result of strong inelastic scattering and is consistent with the linear temperature dependence of the dc conductivity. However, there is no consensus yet for the origin, or even the existence of a separate mid-infrared structure. The work by Rotter *et al.*³ and the previous work by Schlesinger *et al.*⁴ on untwinned YBCO showed that any noticeable MIR structure is absent in the \hat{a} polarization⁵ (CuO chains along the \hat{b} direction), and therefore implied that the CuO chains are solely responsible for this structure. However, substantial additional absorptions starting at $\sim 500 \text{ cm}^{-1}$ and persisting beyond 8000 cm^{-1} are still observed, particularly in reduced- T_c samples.³ Moreover, there appears to be a different doping dependence of the low-energy and the mid-infrared absorption in the La-Sr-Cu-O system.²

The data can be well fitted either by a one-component model using a generalized Drude model with frequency-dependent scattering rate and mass, or by a two-component model simply assuming extra absorption channel(s) besides the free carrier. While the two-component model appears to provide a simple explanation for the data, there is some arbitrariness in the decomposition and no other experimental identification for the source of MIR oscillator(s). The authors of Ref. 3 and 4 showed that $\text{Re}\sigma_a(w)$ can be fitted with a generalized Drude model with frequency-dependent scattering rate and mass at low frequency (up to 3000 cm^{-1}). These fittings suggest that the frequency- and temperature-dependent scattering rate is $\sim kT + \hbar w$ at low frequency. The microscopic origin of the frequency dependence in the parameters of this model is still unclear. Its micro-

scopic justification, for example, with a conventional inelastic scattering of the charge carrier needs an unusually large carrier-boson coupling constant which is not compatible with other transport data (resistivity, for example).

The optical conductivity has been the subject of several finite-cluster exact-diagonalization studies.⁷⁻¹¹ They observed a gap in the optical spectra which scales with the magnetic exchange energy.⁷⁻¹⁰ These studies suggest a possible explanation of the MIR structure within a one band model. A severe limitation of these studies is the very small size of the systems studied.

In a previous publication,^{12,13} we have demonstrated that the large- N slave-boson method applied to the t - J model, in the uniform phase, can accommodate the strong correlation effect with "Fermi-liquid-like" quasiparticle features. The one-particle spectral density¹² shows two main features: (1) the incoherent part of the spectral density spanned over the energy scale of the unrenormalized bandwidth ($\sim t$) and (2) the existence of the strongly renormalized quasiparticle band which satisfies the Luttinger theorem.¹⁴ The results are in qualitative agreement with the finite-cluster exact diagonalization¹⁵ except the details of the discrete peaks which may be intrinsic to the finite size of the clusters studied. Our goal is to see which features of the experiments can be accounted for by our treatment of a one-component model of strongly correlated electrons, and also to understand the trends of the optical absorption with doping and with $\frac{J}{t}$.

Our main findings are the following. First, as in the calculation of the one particle-spectral density, the low-energy spin excitations (chiral fluctuations) govern the low-energy physics and explain the slower decay of the real part of the dynamic conductivity at low frequency. Second, the same mechanism (convolution-type diagram of the quasiparticle and slave boson¹⁶), which contributes to a broad incoherent part in the one-particle spectral density, provides a large incoherent background in the dynamic conductivity. The combination of these two features provides a plausible explanation for the main features of the observed optical conductivity within a

one-component model of strongly correlated electrons. In contrast to the finite-cluster calculations, we do not find a sharp onset of the MIR structure. We explicitly include several vertex corrections together with the various self energy corrections.

We consider the $SU(N)$ generalization of the t - J model in two dimensions defined by

$$H = -\frac{t}{N} \sum_{\text{NN}} (f_{i\sigma}^\dagger b_i f_{j\sigma} b_j^\dagger + \text{H.c.}) + \frac{J}{N} \sum_{\text{NN}} f_{i\sigma}^\dagger f_{i\sigma'} f_{j\sigma'}^\dagger f_{j\sigma}, \quad (1)$$

and the constraint $\sum_{\sigma} f_{i\sigma}^\dagger f_{i\sigma} + b_i^\dagger b_i = N/q_0$ with the sum over repeated $\sigma = 1, \dots, N$ implied. The spin-1/2 t - J model corresponds to the $N = 2$ and $q_0 = 2$ limit of Eq. (1) where b_i is a slave boson introduced to label an empty site and $f_{i\sigma}$ is a fermion carrying the spin quantum number of the projected electron operator $c_{i\sigma}^\dagger = f_{i\sigma}^\dagger b_i$. The partition function of the model is given by $Z = \int D\Delta^\dagger D\Delta D b^\dagger D b D f^\dagger D f D \lambda \exp[-\int_0^\beta L d\tau]$, with

$$L = \sum_i \{ f_{i\sigma}^\dagger [\partial_\tau - \mu] f_{i\sigma} + b_i^\dagger \partial_\tau b_i + i\lambda_i [f_{i\sigma}^\dagger f_{i\sigma} + b_i^\dagger b_i - N/q_0] + \sum_{ij} \{ (N/J) |\Delta_{ij}|^2 - f_{i\sigma}^\dagger f_{j\sigma} [\Delta_{ij} + (1/N) t_{ij} b_j^\dagger b_i] + \text{H.c.} \}, \quad (2)$$

where Δ_{ij} is a Hubbard-Stratanovich field to decouple the spin exchange term and λ_i is a Lagrange multiplier to enforce the local constraint. We work in the radial gauge¹⁷ where the fermion excitations can be identified with the Fermi liquid quasiparticles. In this gauge, the phase of the slave boson ($b_i = r_i e^{i\theta_i}$) has been absorbed in the newly defined quasiparticle operator ($\tilde{f}_{i\sigma} = f_{i\sigma} e^{i\theta_i}$; from now on we will use $f_{i\sigma}$ instead of $\tilde{f}_{i\sigma}$) while making λ_i dynamic field. With the choice of this gauge we can avoid the violation of the Elitzur's theorem¹⁸ because we do not break the local $U(1)$ symmetry explicitly. The Fermi liquid phase of the model¹³ is described by a saddle point uniform in the fields $r_0^2 = N\delta/2$, $\lambda_0 = 4t\Delta/J$, and $\Delta = J/N_s \sum_k \cos k_x f(\epsilon_k)$. It describes quasiparticle with dispersion $E_k = -2W(\cos k_x + \cos k_y) + \lambda_0 - \mu$, $W = \Delta + tr_0^2/N$. The residual interactions are generated by the fluctuating part of the Bose fields: $r_i = r_0(1 + \tilde{r}_i)$, $i\lambda_i = \lambda_0 + i\tilde{\lambda}_i$, and $\Delta_{i,\eta} = \Delta(1 + R_{i,\eta})e^{iA_{i,\eta}}$ with $\eta = x, y$. The effective Lagrangian to quadratic order in the real bose fields $\phi^{1,\dots,6} \equiv (\tilde{r}, \tilde{\lambda}, R_\eta, A_\eta)$ is written as

$$L_{\text{eff}} = \sum_k f_{k\sigma}^\dagger (i\nu_n - E_k) f_{k\sigma} + \sum_{q,k,\alpha} \Lambda_\alpha \phi_q^\alpha f_{k+,\sigma}^\dagger f_{k-,\sigma} + \frac{N}{2} \sum_{q,\alpha,\beta} \phi_q^\alpha D_{\alpha\beta}^{-1} \phi_{-q}^\beta. \quad (3)$$

where $\Lambda_\alpha = [-\frac{2tr_0^2}{N}(\epsilon_{k+} + \epsilon_{k-}), i, -2\Delta \cos k_\eta, 2\Delta \sin k_\eta]$, $\epsilon_{k\pm} = [\cos(k_x \pm \frac{q_x}{2}) + \cos(k_y \pm \frac{q_y}{2})]$ is the fermion-boson coupling vertices, and the inverse boson propa-

gators are given by $D^{-1}(q) = D_0^{-1}(q) + \chi^0(q)$ where D_0^{-1} are the inverse bare boson propagators in Eq. (2) and the χ^0 are fermion polarization bubbles calculated with the vertices.¹³

The total current is the sum of the diamagnetic and paramagnetic components. At zero frequency, and at zero temperature, there is an incomplete cancellation between these terms which gives rise to a δ function peak in the real part of the conductivity.¹⁹ In this paper we calculate the paramagnetic current-current correlation function for nonzero frequency to understand the qualitative feature of experiments and to compare the results with the results of exact diagonalization of finite clusters.

The current operator which couples to the electromagnetic field in the x direction at zero momentum is given by

$$J_x^{\text{para}} = \frac{it}{N} \sum_{i,\sigma} (c_{i,\sigma}^\dagger c_{i+x,\sigma} - c_{i+x,\sigma}^\dagger c_{i,\sigma}) = -\frac{2t}{N} \sum_{k,\sigma} \sin k_x c_{k,\sigma}^\dagger c_{k,\sigma}, \quad (4)$$

where $c_k = \frac{1}{N_{\text{site}}} \sum_q f_{k+q} b_q^\dagger$. And the paramagnetic conductivity is written by

$$\sigma_{\text{para}}(w) = \frac{1}{iw} \int dt \theta(t) \langle [J_x^{\text{para}}(t) J_x^{\text{para}}(0)] \rangle e^{iwt}. \quad (5)$$

In the leading order in the $1/N$ expansion, $\sigma_1(w)$ [$\sigma(w) = \sigma_1(w) + i\sigma_2(w)$] consists of only a diamagnetic δ function peak which carries whole spectral weight. In order to see the interesting inelastic scattering contribution at finite frequency we have to go beyond the leading order calculation. Figure 1 shows all diagrams which

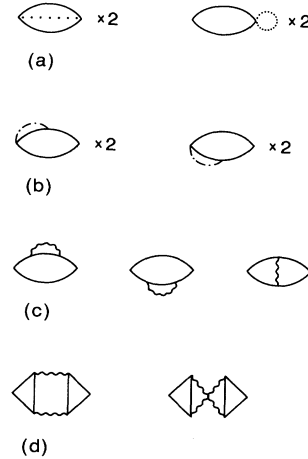


FIG. 1. The next-to-leading order diagrams for the conductivity in $1/N$; (a) convolution type and the corresponding vertex correction, (b) anomalous self-energy correction, (c) ordinary self-energy correction and vertex correction, and (d) two-boson processes. The solid line is for fermion propagator, the dotted line is for slave-boson propagator $D_{\tilde{r}\tilde{r}}$, the dash-dotted line is for $D_{\tilde{r}\alpha}$, and the wiggly line is for all bosonic propagators $D_{\alpha\beta}$. The numbers next to the diagrams are the symmetry factors.

contribute to the conductivity for finite frequency to the next-to-leading order in $1/N$. Because of the nature of the compositeness of the physical electron operator and the condensation of the slave boson new diagrams appear at the next to leading order in $1/N$. Figure 1(a) is the familiar “convolution-type” diagram which gives rise to the incoherent background in the one-particle spectral density and the corresponding vertex-correction diagram which has no contribution at $q = 0$ limit, respectively. Figure 1(b) is the “anomalous self-energy correction” (also shortly called “anomalous”) diagram. Interestingly, these diagrams self-contain the corresponding vertex-correction. This can be seen by a pictorial construction of the vertex correction, i.e., by inserting a photon line to all possible places of the corresponding one-particle propagator. Or, more straightforwardly, when all possible diagrams are exhausted for a given order in any consistent expansion, it automatically includes all necessary vertex- and self-energy corrections. As described in Ref. 12, the physical meaning of the “anomalous self-energy correction” is the dynamic realization to impose the no-double occupancy constraint via fluctuations, thereby representing the strong particle hole asymmetry inherent in strongly correlated electron systems. Figure 1(c) is the standard “self-energy correction” and “vertex correction” diagrams. The numbers next to the diagrams are the symmetry factors. Finally, Fig. 1(d) is the “two-boson” processes, which are the same order as the other one-boson processes in $1/N$ expansion. Therefore, including the two-boson processes is required to satisfy the Ward-Takahashi identity for the f fermion. For the calculation of two-boson processes, we pick up the singularities only coming from two-boson propagators and take only regular parts from fermion loops, which is a reasonable approximation to take account of the most dominant and also physically interesting resonance process in the two-boson diagrams.²⁰ All other diagrams are calculated exactly without approximations except the discretized numerical integrations in momentum and frequency spaces. For most of calculations, 20×20 meshes for one quarter of the Brillouin zone and the frequency discretization $\Delta\omega = 0.04t$ are used.

Now we discuss the results of the calculation. We found that the ordinary self-energy correction diagrams are the main source of absorptions at frequencies below $\sim J$ with smooth but slower decay ($\sim \omega^{-\alpha}$, $\alpha < 2$). Using a numerical experiment, i.e., isolating the contributions of each Bose propagator out of 6×6 propagators, we could identify the low-energy spin fluctuations (or chiral fluctuations in our formalism, i.e., $D_{A_n A_n}$) as the origin of this large scattering at low frequency. The vertex correction does not introduce any qualitatively new feature, but it is the same order of magnitude as the self-energy correction and it is not positive or negative definite. Therefore, it is important to include this diagram for any quantitative comparison with the finite-cluster calculations. The convolution-type diagram provides a large volume of incoherent absorptions extending to the energy scale of the unrenormalized bandwidth of the model ($\sim 2t$). Combining with the other contributions, this provides a plausible explanation for the origin of the extra absorption rang-

ing from MIR frequency to ~ 1 eV (Ref. 3 and 6) in our approach. In contrast to the Holstein process, which is often employed to explain the MIR structure with ordinary bosons (for example, phonons), we do not need an unusually strong quasiparticle-boson coupling to have this large extra absorptions. The anomalous self-energy correction diagram shows the negative absorption power for most of frequencies except $\omega \sim 0$. It is another important strong correlation effect in the slave-boson approach¹² which eliminates the double occupancy. Finally, each of the two-boson processes is of the same order of magnitude as the one-boson vertex correction process. However, there is strong cancellation between direct and exchange processes resulting in a small contribution. The sum of all these contributions gives the real part of the conductivity at finite frequency to the next-to-leading order in the t - J model. More details of each diagrams will be presented elsewhere.²¹

In Fig. 2, we show the conductivity for different dopings ($\delta = 0.2, 0.25$, and 0.3) with $J/t=0.3$. While the t - J model is an oversimplification of the experimentally relevant systems our results seem to provide a natural explanation for the basic features which are observed^{3,4,6} (slower decay at low frequency and the extra absorptions ranging from MIR frequency to ~ 1 eV).

Our results agree with the exact-diagonalization studies⁷⁻¹¹ of small clusters on the energy scale of the broad absorption background.²² However, we do not see any explicit onset of absorptions which is separated from the lower frequency smooth decay, whereas, some finite-cluster calculations⁷⁻¹⁰ show the beginning of a second absorption which is separated from the lowest frequency absorption peak and seems to scale with J . We believe that this is a finite-size effect, and the lowest energy peak and the next absorption peak will merge in the thermodynamic limit to provide the slower decay of the conductivity due to the spin fluctuations, the characteristic energy of which scales with J .

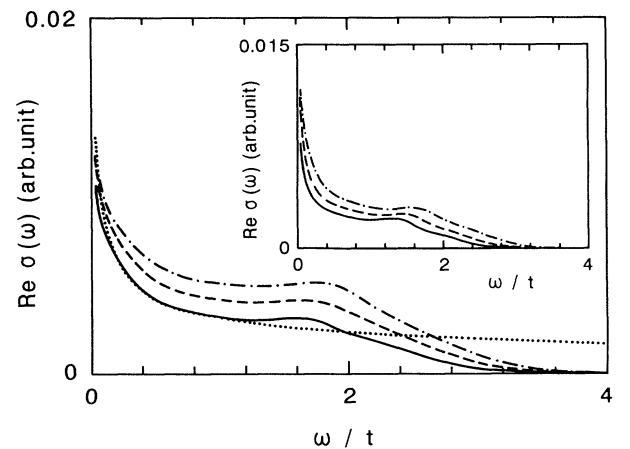


FIG. 2. The conductivity for $J/t=0.3$ and for different dopings: $\delta = 0.2$ (solid), 0.25 (dashed), and 0.3 (dash-dotted), respectively. The dotted curve is the power-law fitting ($\sim \omega^{-0.45}$) for a guide for the eye. Inset: The conductivity for $\delta = 0.2$ and for different exchange couplings: $J/t = 0.1$ (solid), 0.2 (dashed), and 0.3 (dash-dotted), respectively.

The absorption power of the regular part of the conductivity is proportional to the doping rather than the number of particles, consistent with the f -sum rule in the strongly correlated electron system in the vicinity of the Mott-Hubbard transition.²³ For guidance, we show the fitting by power-law curve to the data for $\delta = 0.2$. It decays slower than $\sim \omega^{-1}$, which is not quite compatible with the experiments. However some general trends of the data can be explained by our calculations. It is possible that a partial resummation of diagrams, like the one performed in a previous paper,¹² could result in a better fit to the experiments because the imaginary part of the self energy of the quasiparticle is linear above a very low frequency region. In this case, however, it is not clear how to carry out the vertex corrections consistently. In the inset of Fig. 2, we show the conductivity for different J/t (0.1, 0.2, and 0.3) with a fixed doping $\delta = 0.2$. The results again show that the absorption power increases with increasing J , which is also consistent with the f -sum rule because increasing J increases the total kinetic energy.

Finally, in Fig. 3, we show the one-particle spectral densities calculated next-to-leading order in $1/N$.²⁵ A simple convolution of the spectral densities gives qualitative features of the optical conductivity.

In conclusion, we have calculated the real part of conductivity at finite frequency in the t - J model using the slave-boson large- N technique. The results show that the slow decay at low frequency is due to the strong low energy spin fluctuations extending to $\sim J$, and the extra absorption, extending to the unrenormalized bare energy

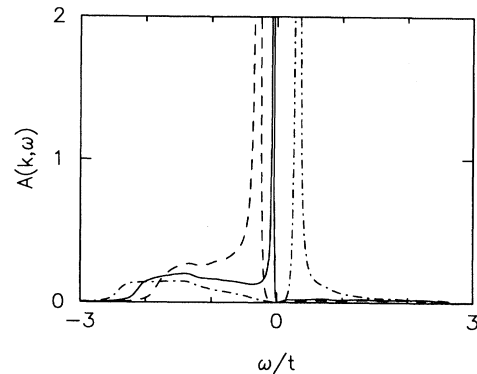


FIG. 3. The one-electron spectral function for $J/t = 0.3$ and $\delta = 0.2$ at $k = 0.87(\pi/2, \pi/2)$ (solid); $k = 0.63(\pi/2, \pi/2)$ (dash); $k = 1.25(\pi/2, \pi/2)$ (chain-dot). The δ function peak at the position of quasiparticle poles is not included.

scale $\sim t$, is from the incoherent motion of the charge carrier. In connection with experiments, it provides a natural explanation for the anomalous behavior of the dynamic conductivity within a one-component model of the strongly correlated electron system. It is also in general agreement with finite-cluster calculations, and gives complementary informations in the thermodynamic limit.

One of the authors (Y.B.) would like to thank P. Fulde and P. Horsch for many useful discussions. He is supported by a grant from the Max-Planck-Gesellschaft. G.K. was supported by NSF Grant No. DMR 92-24000.

¹ G. A. Thomas *et al.*, Phys. Rev. Lett. **61**, 1313 (1988); J. Orenstein *et al.*, Phys. Rev. B **42**, 6342 (1990).

² S. Uchida *et al.*, Phys. Rev. B **43**, 7942 (1991).

³ L. D. Rotter *et al.*, Phys. Rev. Lett. **67**, 2741 (1991).

⁴ Z. Schlesinger *et al.*, Phys. Rev. Lett. **65**, 801 (1990).

⁵ The experiments on Bi-Sr-Ca-Cu-O by Tanner *et al.* (Ref. 6) also show that there is no typical onset of MIR structure above T_c . Nevertheless, these authors argue in favor of the existence of the extra absorptions in the MIR region using the two-component model.

⁶ D. B. Tanner *et al.* (unpublished); also see D. B. Romero *et al.*, Phys. Rev. B **44**, 2818 (1991).

⁷ W. Stephan and P. Horsch, Phys. Rev. B **42**, 8736 (1990).

⁸ A. Moreo and E. Dagotto, Phys. Rev. B **42**, 4786 (1990).

⁹ D. Poilblanc and E. Dagotto, Phys. Rev. B **44**, 466 (1991).

¹⁰ I. Sega and P. Prelovšek, Phys. Rev. B **42**, 892 (1990).

¹¹ C. X. Chen and H. B. Schüttler, Phys. Rev. B **43**, 3771 (1991).

¹² Z. Wang, Yunkyu Bang, and G. Kotliar, Phys. Rev. Lett. **67**, 2733 (1991).

¹³ M. Grilli and G. Kotliar, Phys. Rev. Lett. **64**, 1170 (1990).

¹⁴ J. M. Luttinger, Phys. Rev. **121**, 942 (1961).

¹⁵ W. Stephan and P. Horsch, Phys. Rev. Lett. **66**, 225E (1991); D. Poilblanc, E. Dagotto, and J. Riera, Phys. Rev. B **43**, 7899 (1991).

¹⁶ P. W. Anderson and Z. Zou, Phys. Rev. Lett. **60**, 132 (1988).

¹⁷ N. Read and D. M. Newns, J. Phys. C **16**, 3273 (1983).

¹⁸ S. Elitzur, Phys. Rev. D **12**, 3978 (1975).

¹⁹ W. Kohn, Phys. Rev. **133**, A171 (1964).

²⁰ Utilizing the Cutkosky cut rule we can see that another possible cut would be the process cutting two fermion lines and one boson line near either one of the fermion loops. This process will be proportional to $\Pi_q(w)B_{-q}(w - \Omega)$, where $B_q(w)$ are the spectral functions of the boson propagators and $\Pi_q(w)$ is the spectral function of the standard fermion bubble, whereas our "two boson" approximation will be proportional to $B_q(w)B_{-q}(w - \Omega)$. We neglect the former process since $\Pi_q(w)$ is much smaller than $B_q(w)$, in particular for small doping.

²¹ Yunkyu Bang and G. Kotliar (unpublished).

²² Since our rescaled Hamiltonian has a hopping parameter $\frac{t}{N}$ and N is set to 2 in the physical limit, we should read $t = 2t_0$, where t_0 is the bare hopping parameter.

²³ Since we did not include the Drude weight, this is not a full f -sum rule. However, the numerical study by P. Horsch *et al.* (Ref. 24) shows that the paramagnetic absorption power also shows this trend for small doping.

²⁴ P. Horsch and W. Stephan, in *Proceedings of the International Workshop on the Electronic Properties and Mechanisms in High- T_c Superconductors, Tsukuba, Japan, 1991*, edited by T. Oguchi *et al.* (North-Holland, Amsterdam, 1992).

²⁵ In Ref. 12, the $1/N$ expansion has been made with respect to various self energies. Here we make an expansion directly with the Green function in order to make a comparison with an optical conductivity.